ARTICLE

doi:10.1038/nature18015

Synchronized mitochondrial and cytosolic translation programs

Mary T. Couvillion[1], Iliana C. Soto[1], Gergana Shipkovenska[1] & L. Stirling Churchman[1]

Oxidative phosphorylation (OXPHOS) is a vital process for energy generation, and is carried out by complexes within the mitochondria. OXPHOS complexes pose a unique challenge for cells because their subunits are encoded on both the nuclear and the mitochondrial genomes. Genomic approaches designed to study nuclear/cytosolic and bacterial gene expression have not been broadly applied to mitochondria, so the co-regulation of OXPHOS genes remains largely unexplored. Here we monitor mitochondrial and nuclear gene expression in *Saccharomyces cerevisiae* during mitochondrial biogenesis, when OXPHOS complexes are synthesized. We show that nuclear- and mitochondrial-encoded OXPHOS transcript levels do not increase concordantly. Instead, mitochondrial and cytosolic translation are rapidly, dynamically and synchronously regulated. Furthermore, cytosolic translation processes control mitochondrial translation unidirectionally. Thus, the nuclear genome coordinates mitochondrial and cytosolic translation to orchestrate the timely synthesis of OXPHOS complexes, representing an unappreciated regulatory layer shaping the mitochondrial proteome. Our whole-cell genomic profiling approach establishes a foundation for studies of global gene regulation in mitochondria.

The large majority of cellular energy is produced by oxidative phosphorylation (OXPHOS) complexes within the mitochondrial inner membrane. These complexes consist of a mix of mitochondrial- and nuclear-encoded subunits, requiring the cell to coordinate completely separate gene expression machineries in order to match subunit expression with environmental demands for energy. The mitochondrial gene expression machinery is distinct from its nuclear/cytosolic counterparts, and has also diverged markedly from its bacterial correlates. Transcription is carried out by a single-subunit phage-related RNA polymerase[1] and translation by a dedicated ribosome (the mitoribosome) that is protein-rich compared to cytosolic and bacterial ribosomes[2]. Mitochondrial transcripts are polycistronic and mRNAs have neither 5′ caps nor Shine–Dalgarno sequences. In some species, including *S. cerevisiae*, poly(A) tails are also absent[3]. Mitochondria use modified genetic codes, deciphered by mitochondrial-encoded tRNAs[4]. Most notably, no mitochondrial gene-specific transcription factors have been characterized; instead, mitochondria contain mRNA-specific translational activators, generally present in limiting quantities, that have roles in initiation and\or elongation and, in some cases, in feedback control of OXPHOS complex assembly on subunit translation[5–8]. Thus, the nuclear and mitochondrial genes are expressed by distinct machineries and controlled by disparate regulatory mechanisms. It remains unclear whether these radically different genomes coordinate their gene expression programs during any physiological response when OXPHOS synthesis is required, such as during mitochondrial biogenesis.

OXPHOS mRNAs are not coordinately induced

To analyse OXPHOS expression comprehensively, we used a set of quantitative approaches to monitor the levels and translation of mitochondrial- and nuclear-encoded RNA (Fig. 1a). To induce OXPHOS synthesis, we rapidly shifted *S. cerevisiae* cells from the fermentable carbon source glucose to non-fermentable glycerol, requiring reprogramming of gene expression to adapt to respiratory metabolism[9,10] (Fig. 1b). As expected, steady-state protein levels of both mitochondrial- and nuclear-encoded OXPHOS subunits are induced as cells adapt to respiratory metabolism, and accumulate to high levels in cells undergoing log phase growth in glycerol (Extended Data Fig. 1). Mitochondrial transcripts accumulate in response to the shift[11,12], as do nuclear-encoded OXPHOS mRNAs[13,14], but whether the transcript abundances rise concordantly is not clear. To quantify levels of both nuclear- and mitochondrial-encoded mRNAs we used rRNA depletion, as poly(A) selection would not capture mitochondrial messages, and included spike-in standards to allow quantification across samples. As is observed in most transcriptional programs, nuclear-encoded protein complex components are co-regulated at the RNA level[15] (Extended Data Fig. 2a; full data set provided in Supplementary Table 1). The mitochondrial genome encodes eight major proteins that contribute to dual-origin complexes: the mitoribosome and OXPHOS complexes III–V. The genome also produces low levels of maturases that are required to process *COB* and *COX1* mRNAs (Extended Data Fig. 2b). The nuclear- and mitochondrial-encoded RNAs of the mitoribosome do not change appreciably across the time series, and so by default display similar dynamics (Extended Data Fig. 2c). By contrast, the levels of the nuclear- and mitochondrial-encoded OXPHOS complex RNAs increase during adaptation, but not coordinately (Fig. 1c). Whereas nuclear OXPHOS messages are induced rapidly in response to nutrient shift, mitochondrial OXPHOS messages are induced much more slowly. The difference in induction kinetics may reflect the absence of environment-responsive mitochondrial transcription factors.

Mitochondrial translation is dynamically regulated

Traditionally, mitochondrial translation has been monitored using metabolic labelling after inhibition of cytosolic translation by cycloheximide[16], but this method requires specific buffer conditions and has poor time resolution. Thus, despite the existence of translational activators, it is not known whether translation of mitochondrial mRNAs is differentially regulated under normal physiological conditions, nor whether mitochondrial translation, like cytosolic translation[17], responds rapidly to environmental changes. To quantitatively monitor mitochondrial translation under any growth condition with high time resolution, we re-engineered the ribosome profiling approach originally developed for cytosolic ribosomes[18] through three major modifications. (1) Affinity purification by Flag-tagged mitoribosomal subunits replaced sucrose fractionation to separate 74S mitoribosomes from 80S cytosolic

[1]Department of Genetics, Harvard Medical School, Boston, Massachusetts 02115, USA.

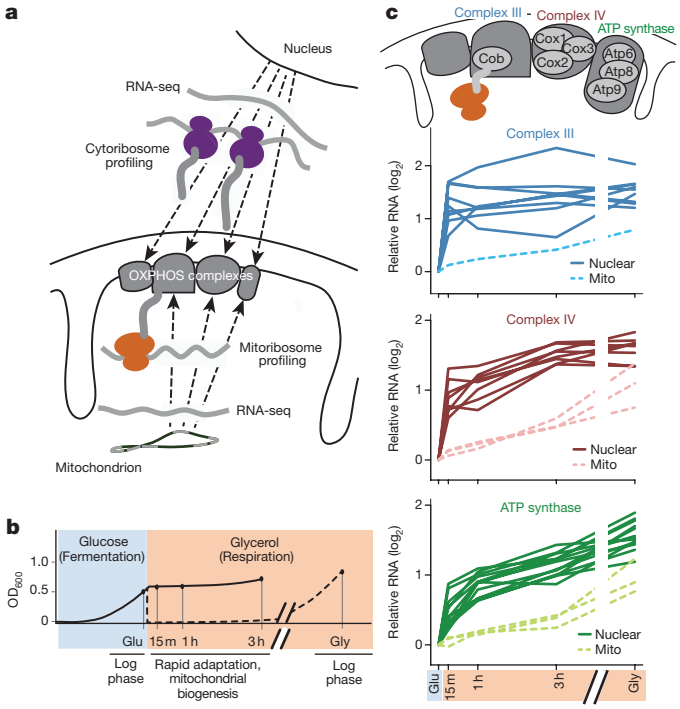

Figure 1 | Expression of dual-origin OXPHOS complexes is induced upon adaptation to respiratory growth. a, Whole-cell genomic profiling approach used to monitor gene expression during mitochondrial biogenesis. Purple, cytoribosomes; orange, mitoribosomes. **b**, Experimental setup to rapidly induce respiratory adaptation. Solid line shows yeast culture grown to log phase in glucose medium and shifted to glycerol medium, where it is cultured for an additional 3 h. Dotted line shows parallel culture that is diluted and incubated for about 16 h for log-phase respiratory growth. **c**, Schematic of the mitochondrial (mito)-encoded proteins of each OXPHOS complex (top), and line plots showing induction kinetics for mRNAs encoding each subunit of the OXPHOS complexes (bottom). Solid lines, nuclear-encoded mRNAs; dotted lines, mito-encoded mRNAs.

ribosomes (cytoribosomes) (Extended Data Fig. 3a–d). (2) Lysis and buffer conditions were optimized to solubilize the membrane-associated mitoribosomes while maintaining subunit association (Extended Data Fig. 3c, d). Although mitoribosome footprints have been captured previously[19], mitoribosomes have strongly altered sensitivity to ionic composition compared to cytoribosomes, and efficient purification of intact mitoribosomes requires optimized conditions[20]. (3) Size selection of footprints was modified as we found mitoribosome-protected fragments are around 38 nucleotides (Fig. 2b, c), in contrast to the ~28-nucleotide cytoribosome-protected fragments[21]. These adaptations enabled the quantitative capture of mitoribosome footprints (Fig. 2a and Extended Data Fig. 4a).

Our approach resulted in reads mapping precisely to all known open reading frames of the 86-kb mitochondrial genome (Fig. 2d, e). Mapped reads show 3-nucleotide periodicity (Extended Data Fig. 4b) and reproducibility is high between biological replicates at the nucleotide level ($r = 0.96$ for reads per million (RPM) values) and at the gene level ($r = 0.9998$ for reads per kilobase of transcript per million mapped reads (RPKM) values; Extended Data Fig. 4c). We found mitochondrial translation inhibitors unnecessary when cells were rapidly collected and lysed while frozen (Extended Data Fig. 4d). Finally, mitoribosome profiling in a strain without the *COX2* translational activator, Pet111, showed a lack of footprint reads mapping to *COX2* (Fig. 2d), confirming genetic evidence that Pet111 affects translation initiation[22].

We applied mitoribosome profiling to cells undergoing respiratory adaption, revealing that mitochondrial-encoded proteins are indeed differentially synthesized during OXPHOS biogenesis (Extended Data Fig. 5a and Supplementary Table 2). To isolate translation regulation from changes in RNA transcript levels, we calculated the translation efficiency (footprint RPKM values/RNA-sequencing (RNA-seq) RPKM values) for each message. We found a rapid and reproducible redistribution of mitoribosomes within 15 min of shifting cells into glycerol (Fig. 3a, Extended Data Fig. 6 and Supplementary Table 3), demonstrating that the differential synthesis is due to strong translational regulation. In the early response, mitoribosomes shift from ATP synthase complex mRNAs to complex IV (cytochrome *c* oxidase complex) mRNAs. Furthermore, translation is dynamically regulated throughout

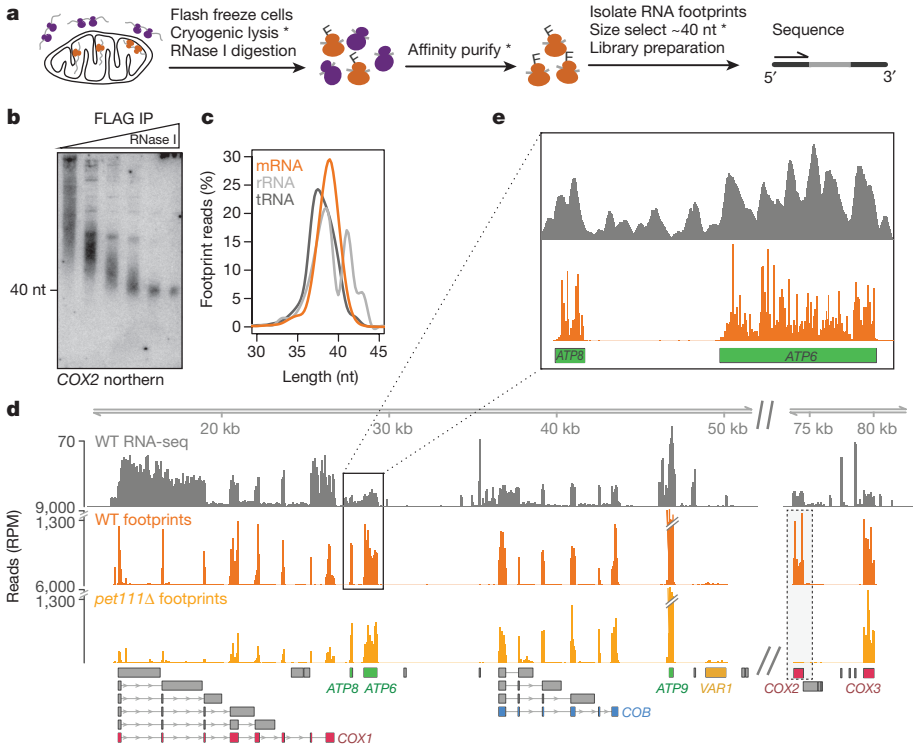

Figure 2 | Mitoribosome profiling provides a genome-wide readout of mitochondrial translation. a, Schematic of mitoribosome profiling protocol. Asterisks denote steps in which major modifications were required to capture mitoribosome footprints rather than cytoribosome footprints. **b**, RNase I titration (0, 50, 125, 250, 500, and 1,000 U ml^{-1}) followed by mitoribosome immunoprecipitation (IP) via MrpS17–Flag. For gel source data, see Supplementary Fig. 1. nt, nucleotides. **c**, Length distribution for mitoribosome profiling reads that map to mitochondrial-encoded mRNA in comparison to contaminating reads that map to rRNA or tRNA. **d**, Genome-wide view of mitochondrial open reading frames (ORFs) with mapped RNA-seq reads and mitoribosome profiling footprint reads (inferred A site). Lack of *COX2*-mapped reads in the *pet111Δ* strain is highlighted. Major ORFs are coloured. Grey annotations are maturase genes (note low level of translation) and tRNA genes. **e**, Expanded view of the region encoding the polycistronic *ATP8*/*ATP6* transcript.

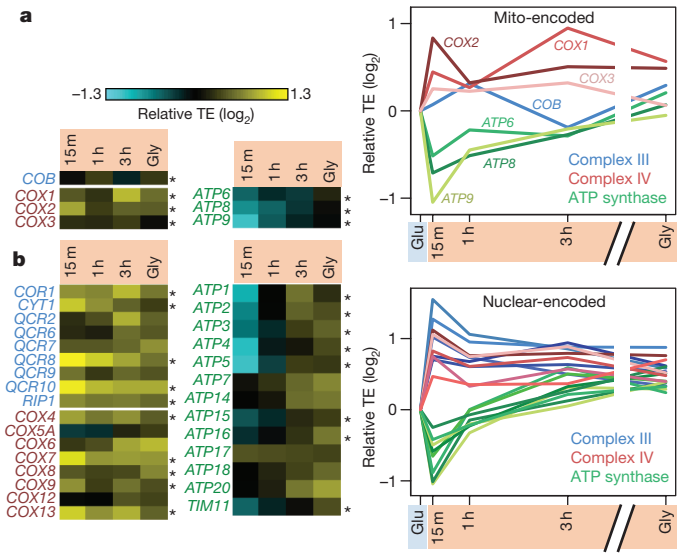

Figure 3 | Mitochondrial and cytosolic translation of OXPHOS mRNAs is rapidly and synchronously regulated. a, **b**, Fold changes in translation efficiency (TE) compared to log-phase glucose growth for the OXPHOS subunits synthesized in mitochondria (**a**; values are averages of two experiments) and the cytosol (**b**). Asterisks on heat maps indicate the subunits shown in the line plots.

the adaptation program; ATP synthase translation recovers over time, *COB* translation is not fully induced until 1 h and *COX1* translation is not fully induced until 3 h. Thus, in contrast to the transcription of mitochondrial-encoded genes, mitochondrial translation is dynamically and differentially regulated.

Translation is coordinated across compartments

To determine whether cytosolic translation is coordinated with the rapid shift in mitochondrial translation efficiencies, we determined the relative synthesis and translation efficiencies for all cytosolic transcripts across our experimental conditions using cytoribosome profiling (Supplementary Tables 4 and 5; representative library characteristics shown in Extended Data Fig. 4a, b). Abrupt transfer from a fermentable to a non-fermentable carbon source results in a transient reduction in cytosolic translation[17] (Extended Data Fig. 7), but select transcripts escape this reduction and are preferentially translated to produce proteins that are required for cell survival under the new conditions[23]. As expected, synthesis of all OXPHOS subunits increases as cells adapt to respiratory growth (Extended Data Fig. 5b); this increase is likely to be driven by the large-scale increase in RNA transcript levels that occurs immediately after carbon source shift. Remarkably, after normalizing for these RNA changes, the pattern of translational regulation of nuclear-encoded OXPHOS subunits is the same as for their mitochondrial-encoded counterparts (Fig. 3b). Within 15 min of nutrient shift, actively translating cytoribosomes markedly redistribute from ATP synthase mRNAs to complex III and complex IV mRNAs. Despite the double membrane separating cytoribosomes and mitoribosomes and a lack of any shared components, translation regulation of OXPHOS subunits is synchronized across cellular compartments.

Translation systems communicate unidirectionally

It is unclear whether communication between the two pools of ribosomes ensures the synchronized regulation of OXPHOS mRNAs, or whether each reacts independently to environmental signals. When mitochondria are isolated from cytosolic factors by treatment with an uncoupler (carbonyl cyanide *m*-chlorophenyl hydrazone (CCCP), which blocks mitochondrial import (Extended Data Fig. 8a)), mitochondrial translation is inhibited across all transcripts, independent of cytosolic translation and carbon source (Extended Data Fig. 8b–e and data not shown). Consistently, *in organello* mitochondrial translation is repressed unless the purified mitochondria are charged with a mixture of amino acids and nucleotides[24].

To determine directly whether communication occurs between the two translation systems, we specifically inhibited cytosolic translation with cycloheximide (CHX)[25] and observed the effect on mitochondrial translation (Fig. 4a–c and Extended Data Fig. 8b). CHX treatment does not affect mitochondrial mRNA levels (Extended Data Fig. 8c), and cells remain viable through the treatment course (Extended Data Fig. 8d). Upon complete inhibition of cytosolic translation, translation of each other during this time period (Fig. 1c). Values in **b** are averages of two experiments. See Source Data for range values. **d**, **e**, Fold changes in translation efficiency of nuclear-encoded OXPHOS subunits measured by cytoribosome profiling (**d**) without (−Pent) or with (+Pent) inhibition of mitochondrial translation, and in ρ^0 cells (**e**). The subset of OXPHOS subunits shown is the same as that shown in line plots in Fig. 3b.

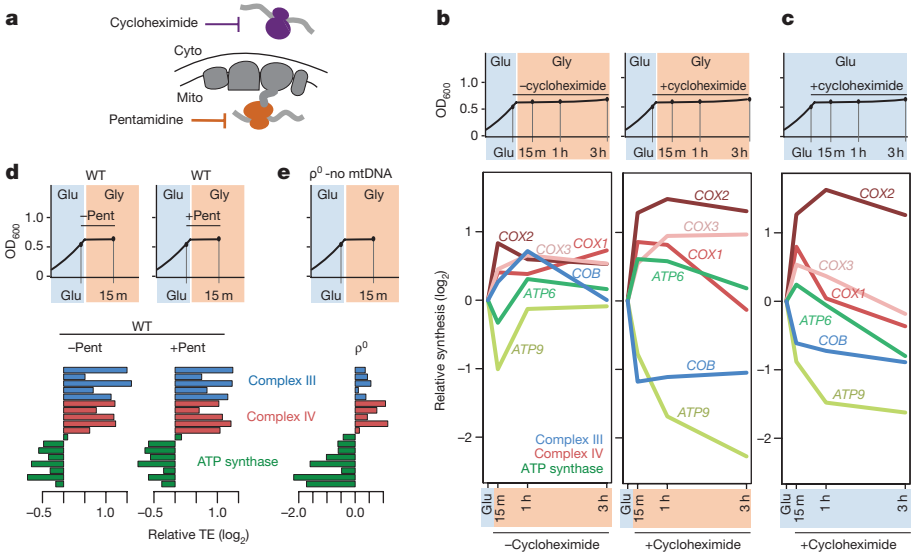

Figure 4 | Communication between translation systems is unidirectional. a, Schematic depicting action of drugs. **b**, **c**, Mitochondrial translation response, measured by northern blotting for footprints (Extended Data Fig. 8b), to cytosolic translation inhibition by CHX with (**b**) or without (**c**) carbon source shift. Note relative synthesis is a good proxy for translation efficiency (compare −CHX to Fig. 3a) because levels of mitochondrial mRNAs do not change substantially relative to

mitochondrial messages is differentially affected: some messages gain translational capacity and others lose it (Fig. 4b). Further, there is a decrease in the dynamics at later time points, with only minor changes occurring after the initial response; this suggests that ongoing cytosolic translation is important for changes in mitochondrial translation over the course of adaptation. Aside from *COB* and *ATP6*, CHX treatment does not substantially alter the rapid (15 min) mitochondrial translational response to a nutrient shift. Surprisingly, CHX treatment influences mitochondrial translation in a similar way even when no change in carbon source occurs (Fig. 4c). Thus, the early change in mitochondrial translation does not occur directly in response to environmental inputs, but rather is a reaction to the transient inhibition of cytosolic translation.

The ability of CHX to prevent translation of *COB* indicates that *COB* translation requires one or more newly synthesized cytosolic products that escape the global stress-induced inhibition of translation. Indeed, the synthesis of two *COB* translational activators, Cbp6 and Cbs2, is increased by nearly fourfold and sixfold, respectively, upon nutrient shift (Extended Data Fig. 8f). Consistent with the gain of *ATP6* translational capacity after treatment with CHX, the *ATP8*/*ATP6* transcript is the only one that has been found to have a translational repressor[26]. These results suggest that cytosolic translational control of translational activators contributes to the orchestration of mitochondrial OXPHOS protein synthesis.

Having established that the synchronization of translational programs is actively controlled by cytosolic translation, we next investigated whether communication between the cytosol and mitochondria is unidirectional or bidirectional. We focused on the early response (15 min after nutrient shift), when translational changes are maximal (Fig. 3b) and any secondary responses should be minimized. When mitochondrial translation was specifically inhibited using pentamidine[27,28] (Fig. 4a and Extended Data Fig. 9a, left panel), ribosome profiling revealed that cytoribosomes respond to the nutrient shift independently of mitochondrial translation (Fig. 4d and Extended Data Fig. 9b). To test the possibility that the cytosolic translation response on OXPHOS mRNAs results from feedback from alterations in membrane potential or the OXPHOS complexes themselves rather than mitochondrial translation, we created a ρ^0 yeast strain (Extended Data Fig. 10a, b). In this strain, which completely lacks mitochondrial DNA, mitochondrial translation, and functional OXPHOS complexes (Extended Data Fig. 9a, right panel), the nutrient shift-induced cytosolic translation response on OXPHOS mRNAs is maintained (Fig. 4e and Extended Data Fig. 9c). Thus, the synchronization of translation is facilitated through unidirectional communication from cytosolic to mitochondrial ribosomes.

Discussion

Translational reprogramming allows rapid changes in protein synthesis and conservation of cellular resources by focusing the expensive process of translation to where it is needed most[29–31]. The preference for synthesis of complex III and IV subunits during adaptation to changes in carbon source may reflect the possibility that these subunits are present in fermenting cells at lower levels than ATP synthase, which functions in reverse in the absence of the electron transport chain to maintain the mitochondrial inner membrane potential[2]. The core subunits of complexes III and IV (Cob and Cox1, respectively), are translationally upregulated at later time points compared to the early response at 15 min for the majority of subunits, probably owing to feedback mechanisms that couple their translation to assembly of their respective complexes[32,33]. Thus, the synchronized translation could serve in part to maximize the efficiency of OXPHOS complex assembly and to limit nonproductive or harmful off-target interactions. Important goals for future studies include unravelling the roles of translation activators and other factors in mediating this synchronized response, and analysing metazoan systems in which some mitochondrial gene regulatory mechanisms have diverged from those found in yeast[3]. We expect that the whole-cell genomic profiling approach described here will usher in an era of global gene expression analyses that will shed light on many aspects of mitochondrial biology in health and disease.

Online Content Methods, along with any additional Extended Data display items and Source Data, are available in the online version of the paper; references unique to these sections appear only in the online paper.

Received 29 October 2015; accepted 18 April 2016.
Published online 11 May 2016.

1. Masters, B. S., Stohl, L. L. & Clayton, D. A. Yeast mitochondrial RNA polymerase is homologous to those encoded by bacteriophages T3 and T7. *Cell* **51,** 89–99 (1987).
2. Faye, G. & Sor, F. Analysis of mitochondrial ribosomal proteins of *Saccharomyces cerevisiae* by two dimensional polyacrylamide gel electrophoresis. *Mol. Gen. Genet.* **155,** 27–34 (1977).
3. Kehrein, K., Bonnefoy, N. & Ott, M. Mitochondrial protein synthesis: efficiency and accuracy. *Antioxid. Redox Signal.* **19,** 1928–1939 (2013).
4. Bonitz, S. G. *et al.* Codon recognition rules in yeast mitochondria. *Proc. Natl Acad. Sci. USA* **77,** 3167–3170 (1980).
5. Costanzo, M. C. & Fox, T. D. Control of mitochondrial gene expression in *Saccharomyces cerevisiae*. *Annu. Rev. Genet.* **24,** 91–113 (1990).
6. Green-Willms, N. S., Butler, C. A., Dunstan, H. M. & Fox, T. D. Pet111p, an inner membrane-bound translational activator that limits expression of the *Saccharomyces cerevisiae* mitochondrial gene COX2. *J. Biol. Chem.* **276,** 6392–6397 (2001).
7. Herrmann, J. M., Woellhaf, M. W. & Bonnefoy, N. Control of protein synthesis in yeast mitochondria: the concept of translational activators. *Biochim. Biophys. Acta* **1833,** 286–294 (2013).
8. Müller, P. P. *et al.* A nuclear mutation that post-transcriptionally blocks accumulation of a yeast mitochondrial gene product can be suppressed by a mitochondrial gene rearrangement. *J. Mol. Biol.* **175,** 431–452 (1984).
9. Fraenkel, D. G. *Yeast Intermediary Metabolism* (Cold Spring Harbor Press, 2011).
10. Kuhn, K. M., DeRisi, J. L., Brown, P. O. & Sarnow, P. Global and specific translational regulation in the genomic response of *Saccharomyces cerevisiae* to a rapid transfer from a fermentable to a nonfermentable carbon source. *Mol. Cell. Biol.* **21,** 916–927 (2001).
11. Amiott, E. A. & Jaehning, J. A. Mitochondrial transcription is regulated via an ATP "sensing" mechanism that couples RNA abundance to respiration. *Mol. Cell* **22,** 329–338 (2006).
12. Mueller, D. M. & Getz, G. S. Steady state analysis of mitochondrial RNA after growth of yeast *Saccharomyces cerevisiae* under catabolite repression and derepression. *J. Biol. Chem.* **261,** 11816–11822 (1986).
13. DeRisi, J. L., Iyer, V. R. & Brown, P. O. Exploring the metabolic and genetic control of gene expression on a genomic scale. *Science* **278,** 680–686 (1997).
14. Roberts, G. G. & Hudson, A. P. Transcriptome profiling of *Saccharomyces cerevisiae* during a transition from fermentative to glycerol-based respiratory growth reveals extensive metabolic and structural remodeling. *Mol. Genet. Genomics* **276,** 170–186 (2006).
15. Eisen, M. B., Spellman, P. T., Brown, P. O. & Botstein, D. Cluster analysis and display of genome-wide expression patterns. *Proc. Natl Acad. Sci. USA* **95,** 14863–14868 (1998).
16. Fox, T. D. *et al.* Analysis and manipulation of yeast mitochondrial genes. *Methods Enzymol.* **194,** 149–165 (1991).
17. Ashe, M. P., De Long, S. K. & Sachs, A. B. Glucose depletion rapidly inhibits translation initiation in yeast. *Mol. Biol. Cell* **11,** 833–848 (2000).
18. Ingolia, N. T., Ghaemmaghami, S., Newman, J. R. & Weissman, J. S. Genome-wide analysis *in vivo* of translation with nucleotide resolution using ribosome profiling. *Science* **324,** 218–223 (2009).
19. Rooijers, K., Loayza-Puch, F., Nijtmans, L. G. & Agami, R. Ribosome profiling reveals features of normal and disease-associated mitochondrial translation. *Nature Commun.* **4,** 2886 (2013).
20. Vignais, P. V., Stevens, B. J., Huet, J. & Andre, J. Mitoribosomes from *Candida utilis*. Morphological, physical, and chemical characterization of the monomer form and of its subunits. *J. Cell Biol.* **54,** 468–492 (1972).
21. Wolin, S. L. & Walter, P. Ribosome pausing and stacking during translation of a eukaryotic mRNA. *EMBO J.* **7,** 3559–3569 (1988).
22. Poutre, C. G. & Fox, T. D. *PET111*, a *Saccharomyces cerevisiae* nuclear gene required for translation of the mitochondrial mRNA encoding cytochrome *c* oxidase subunit II. *Genetics* **115,** 637–647 (1987).
23. Simpson, C. E. & Ashe, M. P. Adaptation to stress in yeast: to translate or not? *Biochem. Soc. Trans.* **40,** 794–799 (2012).
24. Poyton, R. O., Bellus, G., McKee, E. E., Sevarino, K. A. & Goehring, B. *In organello* mitochondrial protein and RNA synthesis systems from *Saccharomyces cerevisiae*. *Methods Enzymol.* **264,** 36–42 (1996).
25. Lamb, A. J., Clark-Walker, G. D. & Linnane, A. W. The biogenesis of mitochondria. 4. The differentiation of mitochondrial and cytoplasmic protein synthesizing systems *in vitro* by antibiotics. *Biochim. Biophys. Acta* **161,** 415–427 (1968).
26. Rak, M. *et al.* Regulation of mitochondrial translation of the *ATP8/ATP6* mRNA by Smt1p. *Mol. Biol. Cell* (2016).
27. Sun, T. & Zhang, Y. Pentamidine binds to tRNA through non-specific hydrophobic interactions and inhibits aminoacylation and translation. *Nucleic Acids Res.* **36,** 1654–1664 (2008).

28. Zhang, Y., Bell, A., Perlman, P. S. & Leibowitz, M. J. Pentamidine inhibits mitochondrial intron splicing and translation in *Saccharomyces cerevisiae*. *RNA* **6,** 937–951 (2000).
29. Liu, B. & Qian, S. B. Translational reprogramming in cellular stress response. *Wiley Interdiscip. Rev. RNA* **5,** 301–315 (2014).
30. Pavlov, M. Y. & Ehrenberg, M. Optimal control of gene expression for fast proteome adaptation to environmental change. *Proc. Natl Acad. Sci. USA* **110,** 20527–20532 (2013).
31. Sonenberg, N. & Hinnebusch, A. G. Regulation of translation initiation in eukaryotes: mechanisms and biological targets. *Cell* **136,** 731–745 (2009).
32. Gruschke, S. *et al.* The Cbp3-Cbp6 complex coordinates cytochrome *b* synthesis with bc_1 complex assembly in yeast mitochondria. *J. Cell Biol.* **199,** 137–150 (2012).
33. Perez-Martinez, X., Butler, C. A., Shingu-Vazquez, M. & Fox, T. D. Dual functions of Mss51 couple synthesis of Cox1 to assembly of cytochrome c oxidase in *Saccharomyces cerevisiae* mitochondria. *Mol. Biol. Cell* **20,** 4371–4380 (2009).

Supplementary Information is available in the online version of the paper.

Acknowledgements We thank F. Winston, T. Fox, G. Brar and members of the Churchman lab for advice and discussions; members of the O'Shea, Novina, and Springer labs for use of equipment and advice; and M. Hickman and D. Botstein for sharing the *HAP1*$^+$ strain. Research supported by a Damon Runyon Cancer Research Foundation Frey Award (to L.S.C.), a Burroughs Wellcome Fund Career Award at the Scientific Interface (to L.S.C.), an Ellison Medical Foundation New Scholar in Aging Award (to L.S.C.), the National Institutes of Health F32 (to M.T.C.), and a Boehringer Ingelheim Fonds PhD Fellowship (to G.S.).

Author Contributions M.T.C. and L.S.C. designed the research and wrote the manuscript. M.T.C. conducted the experiments with help from I.C.S. who performed mitoribosome profiling with drug treatments, and G.S., who created and performed mitoribosome profiling on the *pet111*Δ strain. M.T.C. analysed the data. All authors discussed the results and commented on the manuscript.

Author Information All data are deposited in Gene Expression Omnibus (accession number GSE74454). Reprints and permissions information is available at www.nature.com/reprints. The authors declare no competing financial interests. Readers are welcome to comment on the online version of the paper. Correspondence and requests for materials should be addressed to L.S.C. (churchman@genetics.med.harvard.edu).

Reviewer Information *Nature* thanks P. Van Damme and the other anonymous reviewer(s) for their contribution to the peer review of this work.

METHODS

No statistical methods were used to predetermine sample size. The experiments were not randomized and the investigators were not blinded to allocation during experiments or outcome assessment.

Strain construction, growth conditions, and petite frequency analysis. To ensure a robust and physiological response, we modified the S288c background typically used for genomic studies to make it amenable to mitochondrial studies by correcting the *HAP1* mutation that leads to lower mitochondrial biomass production[34,35] and creating a point change to restore a conserved amino acid that is important for the fidelity of the mitochondrial DNA (mtDNA) polymerase[36,37]. These modifications markedly reduced the frequency of mtDNA loss (Extended Data Fig. 3b). S288c derivative DBY12045 (*MAT***a** *HAP1*$^{+}$ *GAL2*$^{+}$ *ura3*Δ*0 MIP1[S]*) was a gift from M. Hickman and D. Botstein. It was modified by generating a single point change using a loopout strategy to create *MIP1[S]*^{A661T}, repairing a strictly conserved threonine that is mutated in S288c and is responsible for the increased rate of mitochondrial mutations in this strain[36]. Epitope-tagged proteins were expressed from their endogenous loci and generated using a 'scarless' loopout strategy[38,39]. Deletion of *PET111* was performed using the *delitto perfetto* approach[40]. For ρ^0 strain generation, mtDNA loss was induced by overnight growth in 10 μg ml^{-1} ethidium bromide at 25 °C.

Petite frequency was assayed essentially as described[41]. Briefly, fresh colonies from yeast extract peptone dextrose (YPD; 2% glucose) plates were resuspended and plated at low density on YPDG (0.1% glucose, 3% glycerol). 'Petite' and 'grande' colonies were counted after 5 days of growth at 30 °C.

Yeast strains were grown in YP (1% yeast extract, 2% peptone) medium, pH 5.0, supplemented with 2% glucose (Glu) or 3% glycerol (Gly) as indicated. The *pet111*Δ strain is respiratory-deficient and was therefore grown in YPGal (2% galactose) instead of YPGly. Controlling the pH of the medium is essential for consistent growth on glycerol. Overnight liquid YPD cultures were grown to saturation and used to inoculate fresh medium to $OD_{600} \leq 0.06$. Cultures were grown at 30 °C until OD_{600} reached 0.6–0.8. For rapid media transfer, cultures were harvested by filtration, rinsed once in YP (containing drug as indicated), and scraped off the filter into fresh medium. All media and flasks were pre-warmed. Where indicated, CHX (Sigma) was used in cultures at a final concentration of 100 μg ml^{-1}, pentamidine (Sigma) at 10 μM, and CCCP (Sigma) at 40 μM.

FACS analysis. Yeast cultures were grown until they reached $OD_{600} = 0.5$ in YP (1% yeast extract, 2% peptone), pH 5.0 supplemented with 2% glucose. Where indicated, cells were treated with 40 μM CCCP for 2 or 5 min. After treatment, the drug was washed off with 1× PBS and cells were diluted to 10^6 cells per ml in 1× PBS. Where indicated, diluted cells were treated with tetramethylrhodamine (TMRM) at 1 μM for 30 min. Cells were washed twice, resuspended in 1× PBS to a final concentration of 10^6 ml^{-1} and loaded into 96-well culture plates (CellTreat). FACS analysis was performed using a Stratedigm 1000 instrument. Emission wavelengths were recorded at 586 nm. Histograms were generated using FlowJo software.

General nucleic acid and protein methods. For footprint detection by northern blotting, RNA was isolated from purified mitoribosomes (Flag eluate) and loaded on a 15% polyacrylamide TBE-urea gel. After transfer to nylon (Hybond N+), blots were probed at room temperature with internally labelled random hexamer-primed DNA fragments synthesized from 200–500-bp PCR-generated templates. For mRNA detection, RNA was separated on 1.2% formaldehyde agarose and blots were probed at 42 °C. Quantitative PCR (qPCR) was performed using a CFX BioRad Connection qPCR thermocycler with EvaGreen (BioRad) fluorescent dye.

Proteins were resolved before silver staining or western blotting on NuPAGE Novex Bis-Tris gels (Thermo Fisher Scientific). Staining was done with the SilverQuest Silver Staining Kit (Invitrogen) according to the manufacturer's instructions. Antibodies against OXPHOS proteins were purchased from Santa Cruz Biotechnology (anti-Cob, sc-11436) and Abcam Mitosciences (anti-Cox1, ab110270; anti-Cox2, ab110271; anti-Cox4, ab110272). Fluorescently labelled secondary antibodies (IRDye, LI-COR) were detected using the LI-COR Odyssey.

Metabolic labelling was performed essentially as described[42]. Briefly, cultures were grown in YPGal (2% galactose) to log phase, washed and resuspended in potassium phosphate buffer at 30 °C, shaking, for 2 h. Pentamidine was added to 10 μM where indicated and incubation continued for 15 min. To assay mitochondrial translation, CHX was added to 500 μg ml^{-1} for 3 min before addition of ^{35}S-labelled methionine and cysteine mix (Perkin Elmer). Labelling was continued for 20 min at 30 °C. Proteins were TCA precipitated, resolved on 17.5% Tris-glycine polyacrylamide, pH 8.3, and transferred to nitrocellulose. For visualizing cytosolic translation, CHX was omitted and protein samples were diluted 1:15 before loading the gel.

Mitoribosome profiling. Cell culture (400 OD_{600} equivalents) was rapidly harvested by filtration onto 0.45-μm nitrocellulose (Whatman). Cell pellets were flash frozen in liquid nitrogen and combined with 4 ml of frozen lysis buffer (10 mM Tris, pH 8.0, 50 mM NH_4Cl, 10 mM $MgCl_2$, 0.5% lauryl maltoside, 0.25 mM DTT, 1.5× protease inhibitor cocktail (Complete, EDTA-free, Roche)). In optimizing buffer conditions to maintain mitoribosome subunit association, we found the ratio of monovalent to divalent cations to be of vital importance[20]. The frozen cell mixture was pulverized in 50-ml canisters prechilled in liquid nitrogen for six cycles of 3 min each at 15 Hz, on a Retsch MM301 mixer mill. Upon thawing, fresh lysis buffer was added to bring the lysate concentration to 25 OD_{600} equivalents per ml. Lysate was digested for 30 min at 25 °C with 500 U ml^{-1} of recombinant RNase I ($RNase\ I_f$, NEB). The reaction was stopped with 100 U ml^{-1} SUPERase-In (Thermo Fisher Scientific) and clarified by centrifugation at 4 °C at 20,000*g* for 15 min. The supernatant was reserved for immunoprecipitation.

Anti-Flag M2 affinity gel (Sigma) was washed 3× with wash buffer (10 mM Tris pH 8.0, 50 mM NH_4Cl, 10 mM $MgCl_2$, 0.1% Triton X-100), and added to clarified lysate at 12 μl 50% gel slurry per ml. The mixture was rotated end-over-end at 4 °C for 3 h. The affinity gel was washed 3× for 10 min in 10 ml of wash buffer at room temperature, then Flag-tagged protein was eluted by incubation with 200 μg ml^{-1} 3× Flag peptide (Sigma) in 6× volumes affinity gel slurry for 40 min at room temperature. RNA was isolated using phenol/chloroform extraction.

Mitoribosome-protected fragments were isolated by excision of ~36–42-nucleotide fragments from 12% or 15% TBE–urea polyacrylamide gels. Sequencing library preparation was performed through a circular intermediate as described[43], omitting the rRNA depletion step. Sequencing was performed on an Illumina MiSeq system using Reagent Kit v2 or v3. All experiments were performed in biological duplicate and means reported.

Cytoribosome profiling. Cytoribosome profiling for data presented in Fig. 3b and Extended Data Fig. 8f was performed using sucrose density gradients as described[43], except that CHX was omitted from cultures, and frozen cells were pulverized with lysis buffer containing CHX. Cytoribosome profiling for data presented in Fig. 4d, e and Extended Data Fig. 9b, c was performed using 1.0 M sucrose cushions in place of gradients. Sequencing libraries were prepared identically to those for mitoribosome profiling (above). Sequencing was performed on an Illumina NextSeq 500 system. Each experiment presented was performed once as cytoribosome profiling is highly reproducible[44,45]. Additionally, trends are reproducible between experiments performed with density gradients and cushions.

mRNA sequencing. Total RNA was isolated before RNase I digestion from a portion of the thawed lysates described above. ERCC RNA Spike-In Mix (Thermo Fisher Scientific), a mixture of 92 *in vitro* synthesized transcripts, was added in equal volumes across samples that were prepared from equal cell numbers. 50 μg of the total RNA with spike-in mix was digested with 3 U RQ1 RNase-free DNase (Promega) for 30 min at 37 °C. 5 μg of purified RNA was then subjected to rRNA depletion using the Ribo-Zero Magnetic Gold Kit for yeast (Epicentre) according to the manufacturer's instructions.

Sequencing libraries were prepared as above following fragmentation by alkaline hydrolysis in 5 mM Na_2CO_3, 45 mM $NaHCO_3$, 1 mM EDTA, pH 9.3 for 25 min at 95 °C and gel isolation of 30–70-nucleotide fragments unless otherwise noted (Extended Data Fig. 4b). Sequencing was performed on an Illumina NextSeq 500 system. Each experiment was performed once.

Data analysis. Raw sequences were processed by first removing 3′ adaptor sequence using Cutadapt[46] and removing the first nucleotide from the 5′ end of all reads (except where otherwise noted) because we observed, as has been previously reported[43], that this nucleotide frequently represents untemplated addition by reverse transcriptase Supercript III (Thermo Fisher). Next, reads mapping to non-coding RNAs were removed by aligning using Bowtie1 (ref. 47) to a collection of RNA genes downloaded from the *Saccharomyces* Genome Database. Notably, we allowed a 3-nt 3′ mismatch when mapping to tRNAs to account for non-templated CCA addition on mature tRNAs. Remaining reads were then aligned allowing two mismatches to the *S. cerevisiae* genome assembly R64 (UCSC: sacCer3) using Tophat2 (ref. 48). We also aligned separately to the nuclear and mitochondrial genomes to determine the proportions of each library mapping to each.

To determine the A-site position in mitoribosome footprints we observed the first reads mapping to each ORF, which overlap the start codons. Consistently for 36–40-nucleotide reads, the 3′ ends of these reads were 19 nucleotides downstream of the start codon (mitoribosome P site). The 5′ ends were more heterogeneous, depending on length of the read. Thus we assigned A sites for each read as 16 nucleotides from the 3′ end.

RNA-seq normalization to spike-ins was performed by dividing the raw read count at each position by the number of spike-in reads in the library (RPS, reads per spike-in). The number of spike-in reads is a proxy for cell number (see above). RNA-seq reads were also normalized to total nuclear or mitochondrial mRNA mappers, as were cytoribosome profiling and mitoribosome profiling reads, respectively (RPM).

To determine expression values for each gene, RPS or RPM values were summed across ORFs and normalized to ORF length (RPKS or RPKM, respectively; normalized reads per kb). For footprint reads, the first and last five codons were

excluded to remove effects of translation initiation and termination[49]. Translation efficiency was calculated by dividing cytoribosome footprint RPKM values by nuclear-mapping RNA-seq RPKM values and mitoribosome footprint RPKM values by mito-mapping RNA-seq RPKM values.

Scripts for A-site assignment, normalization, translation efficiency calculation, and other text file manipulations were written for Python 2.7.5. Plots and genome browser visualization were generated using R version 3.2.2 and Bioconductor. Heat maps were generated with Matrix2png (http://www.chibi.ubc.ca/matrix2png/).

For analysis of mitoribosome footprints by northern blotting, phosphoimager signals were quantified using ImageJ (http://imagej.nih.gov/) and normalized to the amount of mitoribosome recovered as measured by Mrps17–Flag in elution. Comparisons were made only between samples on the same membrane probed at the same time with the same probe.

34. Ehrenreich, I. M. *et al.* Dissection of genetically complex traits with extremely large pools of yeast segregants. *Nature* **464,** 1039–1042 (2010).
35. Gaisne, M., Becam, A. M., Verdiere, J. & Herbert, C. J. A 'natural' mutation in *Saccharomyces cerevisiae* strains derived from S288c affects the complex regulatory gene *HAP1* (*CYP1*). *Curr. Genet.* **36,** 195–200 (1999).
36. Baruffini, E., Lodi, T., Dallabona, C. & Foury, F. A single nucleotide polymorphism in the DNA polymerase gamma gene of *Saccharomyces cerevisiae* laboratory strains is responsible for increased mitochondrial DNA mutability. *Genetics* **177,** 1227–1231 (2007).
37. Young, M. J. & Court, D. A. Effects of the S288c genetic background and common auxotrophic markers on mitochondrial DNA function in *Saccharomyces cerevisiae*. *Yeast* **25,** 903–912 (2008).
38. Alani, E., Cao, L. & Kleckner, N. A method for gene disruption that allows repeated use of URA3 selection in the construction of multiply disrupted yeast strains. *Genetics* **116,** 541–545 (1987).
39. Moqtaderi, Z. & Struhl, K. Expanding the repertoire of plasmids for PCR-mediated epitope tagging in yeast. *Yeast* **25,** 287–292 (2008).
40. Storici, F. & Resnick, M. A. The delitto perfetto approach to *in vivo* site-directed mutagenesis and chromosome rearrangements with synthetic oligonucleotides in yeast. *Methods Enzymol.* **409,** 329–345 (2006).
41. Dimitrov, L. N., Brem, R. B., Kruglyak, L. & Gottschling, D. E. Polymorphisms in multiple genes contribute to the spontaneous mitochondrial genome instability of *Saccharomyces cerevisiae* S288C strains. *Genetics* **183,** 365–383 (2009).
42. Gouget, K., Verde, F. & Barrientos, A. *In vivo* labeling and analysis of mitochondrial translation products in budding and in fission yeasts. *Methods Mol. Biol.* **457,** 113–124 (2008).
43. Ingolia, N. T., Brar, G. A., Rouskin, S., McGeachy, A. M. & Weissman, J. S. The ribosome profiling strategy for monitoring translation in vivo by deep sequencing of ribosome-protected mRNA fragments. *Nature Protocols* **7,** 1534–1550 (2012).
44. Brar, G. A. *et al.* High-resolution view of the yeast meiotic program revealed by ribosome profiling. *Science* **335,** 552–557 (2012).
45. Ingolia, N. T. Genome-wide translational profiling by ribosome footprinting. *Methods Enzymol.* **470,** 119–142 (2010).
46. Martin, M. Cutadapt removes adaptor sequences from high-throughput sequencing reads. *EMBnet.journal* **17,** 10–12 (2011).
47. Langmead, B., Trapnell, C., Pop, M. & Salzberg, S. L. Ultrafast and memory-efficient alignment of short DNA sequences to the human genome. *Genome Biol.* **10,** R25 (2009).
48. Kim, D. *et al.* TopHat2: accurate alignment of transcriptomes in the presence of insertions, deletions and gene fusions. *Genome Biol.* **14,** R36 (2013).
49. Li, G. W., Burkhardt, D., Gross, C. & Weissman, J. S. Quantifying absolute protein synthesis rates reveals principles underlying allocation of cellular resources. *Cell* **157,** 624–635 (2014).

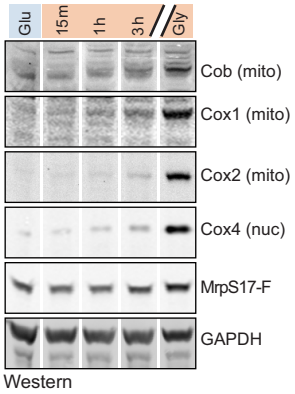

Extended Data Figure 1 | OXPHOS proteins are induced during mitochondrial biogenesis. Western blot analysis of mitochondrial (Cob, Cox1, Cox2) and nuclear (Cox4) OXPHOS proteins compared to Flag-tagged mitoribosome small subunit protein MrpS17. GAPDH was used as a loading control. For gel source data, see Supplementary Fig. 1.

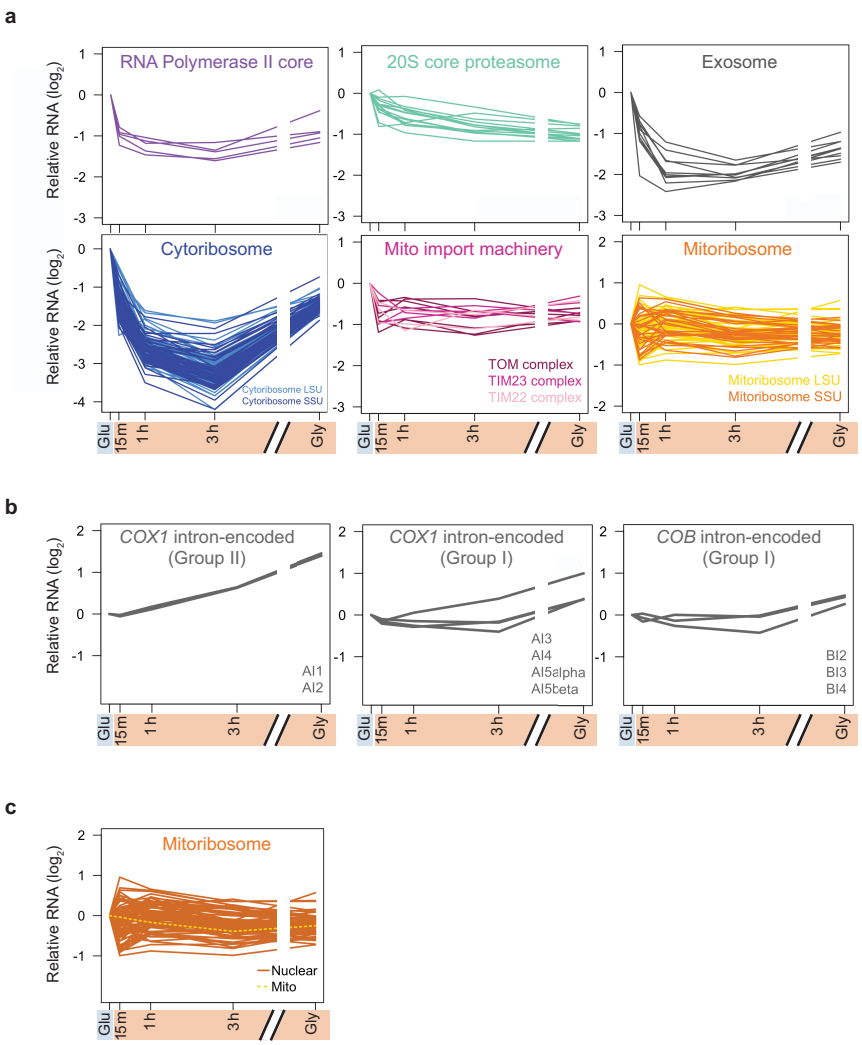

Extended Data Figure 2 | Dynamics of non-OXPHOS RNAs during mitochondrial biogenesis. a–c, RNA levels (reads per kb) normalized to spike-in controls and plotted as fold changes compared to levels in log phase glucose growth for all nuclear-encoded structural components of the complexes shown (**a**); intron-encoded maturases (**b**); and nuclear and mitochondrial-encoded mitoribosome subunits (**c**). To calculate values for maturase transcripts, only reads not overlapping the main ORF (*COX1* or *COB*) were considered. Group II intron splicing intermediates stably accumulate and may not represent translation-competent transcripts.

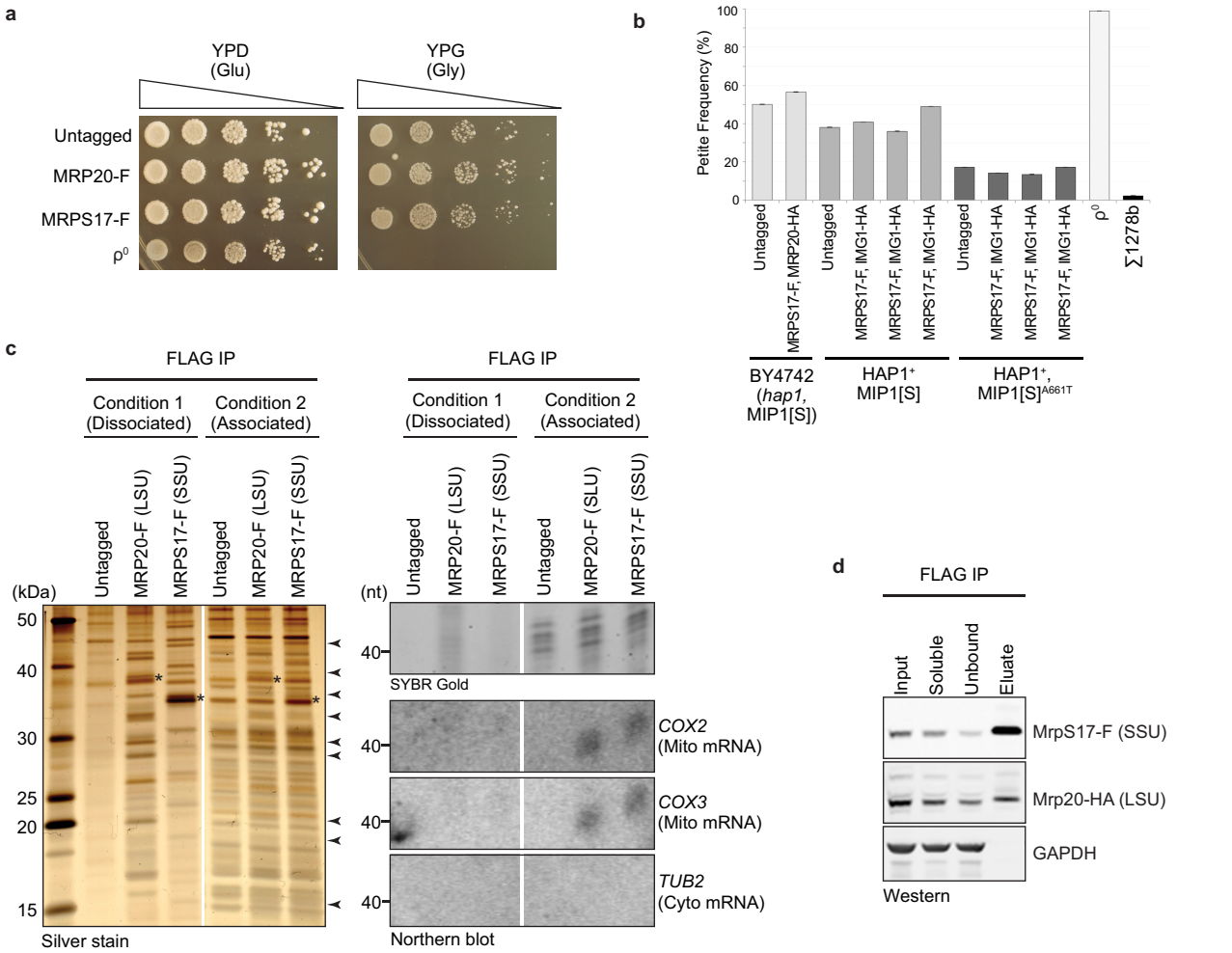

Extended Data Figure 3 | Optimization of affinity purification for intact mitoribosomes. a, Serial dilution spot tests verifying tagged mitoribosome subunits are functional as they support respiratory growth on glycerol (YPG). ρ^0 is a strain without mitochondrial DNA. **b**, Frequency of petite colonies in our corrected S288c strain (see Methods) after growth for 5 days on 0.1% glucose and 3% glycerol. BY4742 is S288c background with designer auxotrophies. Σ1278b is a strain with wild-type *HAP1*, and a high-fidelity allele of *MIP1*, *MIP1[Σ]*, along with other differences compared to S288c. Error bars show variation due to counting, with 175–750 colonies counted for each sample. **c**, Lysis and immunoprecipitation buffer conditions affect mitoribosome subunit association and thus footprint retention. Left: silver staining after immunoprecipitation of the large subunit (LSU) with Mrp20–Flag and of the small subunit (SSU) with Mrps17–Flag in condition 1 (20 mM Tris pH 8.0, 200 mM KCl, 5 mM $MgCl_2$, 0.5% lauryl maltoside), and in condition 2 (10 mM Tris pH 8.0, 50 mM NH_4Cl, 10 mM $MgCl_2$, 0.5% lauryl maltoside). Arrowheads indicate bands that appear in both immunoprecipitations in condition 2 that can be assigned to the LSU or SSU by comparison to condition 1. Asterisks mark the expected mobility of the tagged proteins. Right: northern blotting of the co-purifying RNA in each condition. For gel source data, see Supplementary Fig. 1. **d**, Western blot showing fractions from immunoprecipitation using optimized buffer conditions. Flag immunoprecipitation targeting the mitoribosome SSU co-purifies a haemagglutinin (HA)-tagged LSU protein. For gel source data, see Supplementary Fig. 1.

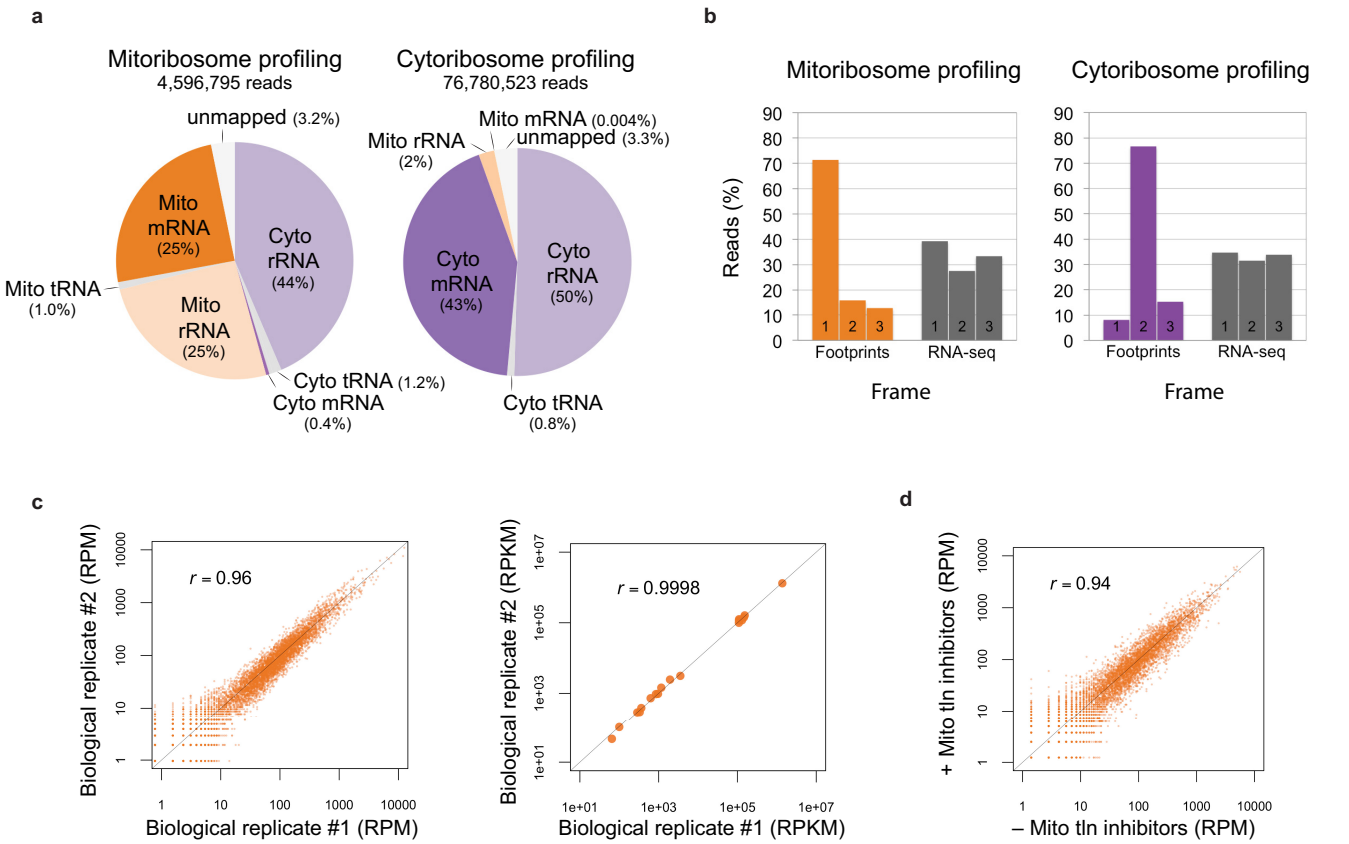

Extended Data Figure 4 | Mitoribosome profiling is robust, reproducible, and does not require translation inhibitors. a, Mapping statistics for representative mitoribosome and cytoribosome profiling libraries from log phase glycerol-grown cells. **b**, Fraction of reads mapping to each frame of mitochondrial ORFs (left) and nuclear ORFs (right) in mitoribosome profiling and cytoribosome profiling data, respectively. RNA-seq reads in the left panel were treated identically to footprint reads, including size selection for library generation. **c**, Reproducibility between biological replicates. Each dot corresponds to the number of reads mapped to a particular position on mRNA (RPM, left), or summed number of reads mapped across each mRNA then normalized to length (RPKM, right). **d**, Reproducibility with and without translation inhibitors thiamphenicol (50 $\mu g\,ml^{-1}$) and GTP analogue GMPPNP (1 mM).

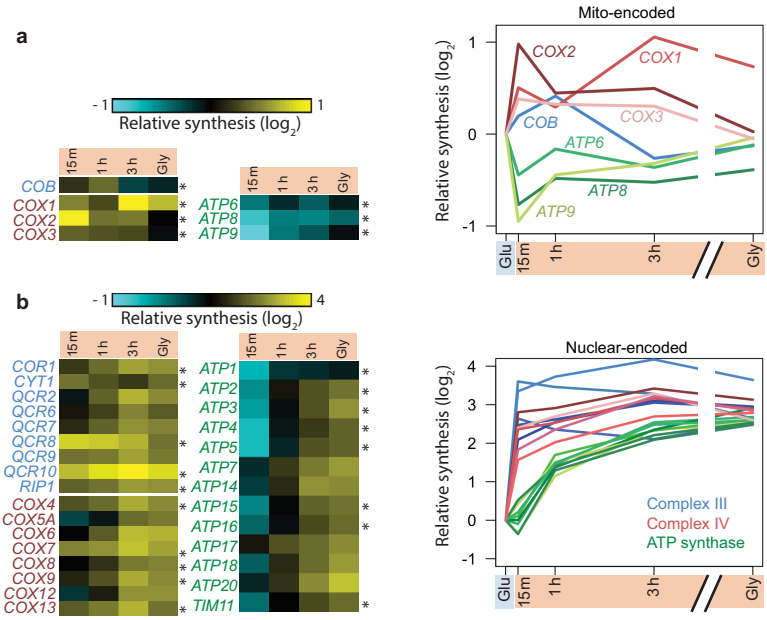

Extended Data Figure 5 | Mitochondrial and cytosolic protein synthesis on OXPHOS mRNAs is rapidly regulated. a, **b**, Fold changes in relative protein synthesis (footprint RPKM values) compared to log phase glucose growth for the OXPHOS subunits synthesized in mitochondria (**a;** values are means of two experiments) and cytosol (**b**). Asterisks on heat maps indicate the subunits shown in the line plots.

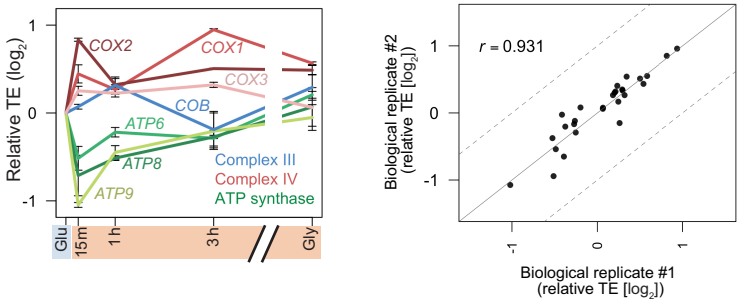

Extended Data Figure 6 | Mitoribosome translation efficiency fold changes are reproducible. Fold change data identical to those shown in Fig. 3a, but including range bars for two experiments performed from independent cultures on different days (left), and fold change translation efficiency data plotted as a scatter with the Pearson correlation coefficient (right). Dotted lines mark twofold difference. RNA-seq data used in calculating translation efficiency are from a single experiment.

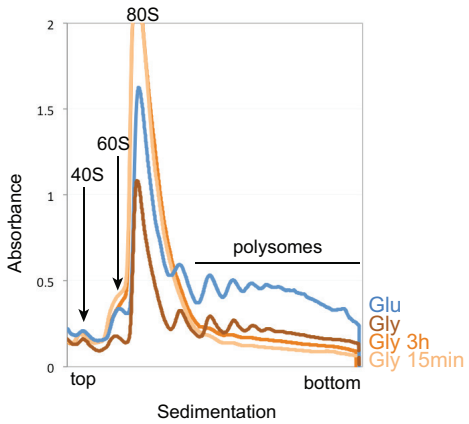

Extended Data Figure 7 | Global translation is transiently inhibited upon shift to glycerol. Polysome profiles from samples used for cytoribosome profiling, but without RNase I treatment. Gradients were loaded with lysate from equal cell numbers, allowing overall ribosome abundances to be compared between samples. Doubling time during log phase is ~1.2 h in glucose and ~3.7 h in glycerol.

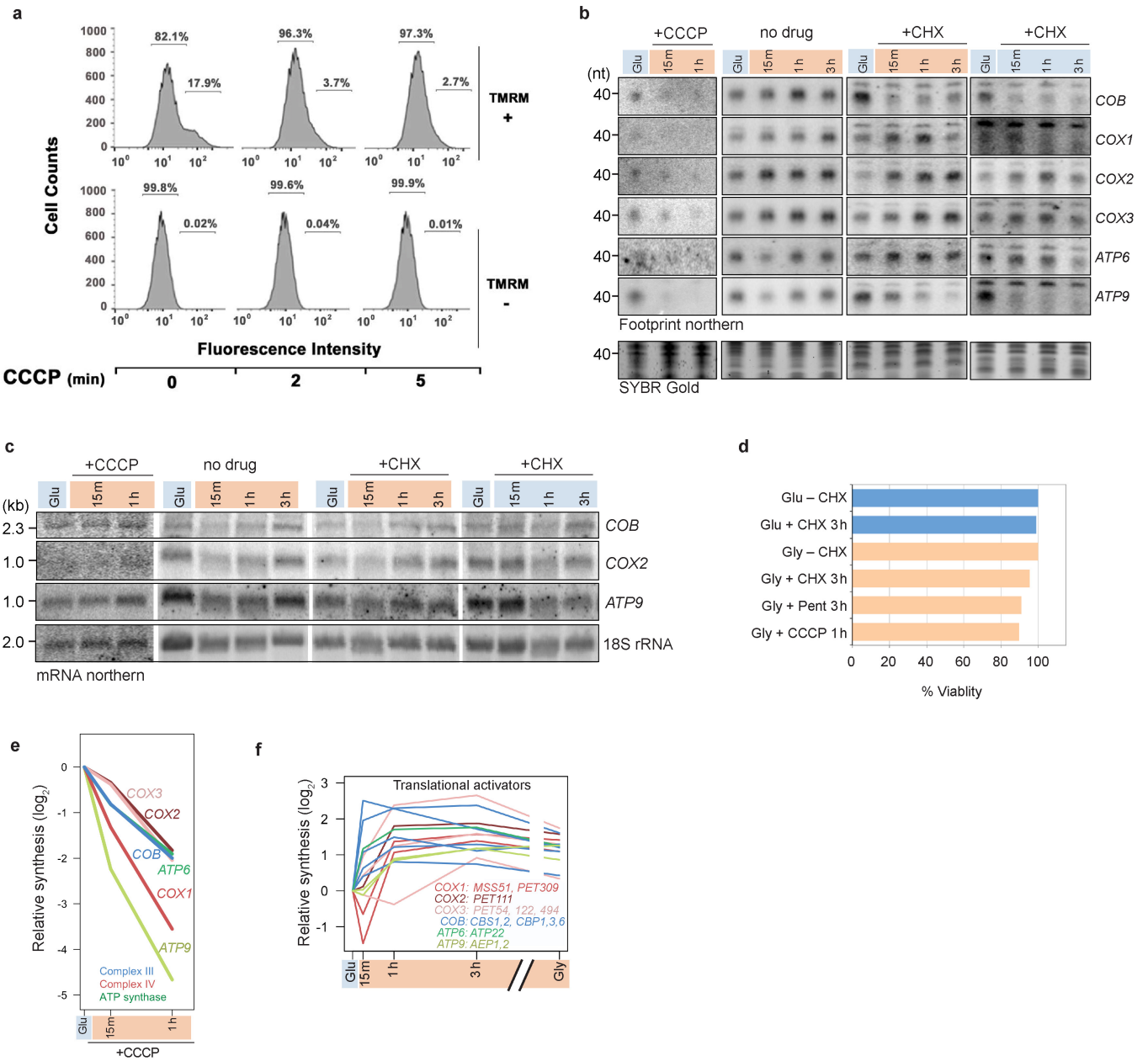

Extended Data Figure 8 | Cytosolic translation controls mitochondrial translation response. a, FACS analysis of yeast cultures treated with CCCP. Wild-type cultures were grown in glucose to mid-log phase and treated with 40 μM CCCP for the indicated times. Mitochondrial membrane potential ($\Delta\Psi$m) was assessed using 1 μM tetramethylrhodamine (TMRM), which is taken up by only a fraction of the cell population (17.9% in this experiment). TMRM accumulates inside negatively charged mitochondria, producing increased fluorescence intensity (10^2). Loss of membrane potential dissipates probe, measured as loss of high-intensity fluorescence. **b**, Representative northern blots for data in Fig. 4b, c and panel **e**. For quantification, northern signals were normalized by relative mitoribosome recovery measured by Mrps17–Flag signal in western blots. For gel source data, see Supplementary Fig. 1. **c**, Northern blotting of total RNA for the indicated transcripts. For gel source data, see Supplementary Fig. 1. **d**, Quantification of viability assay. Cells were grown in YPD (Glu) or YPG (Gly) with or without drug for the time indicated. Cells were washed out of drug and plated on YPD for calculation of colony-forming units. CCCP (40 μM); CHX (100 μg ml^{-1}); pentamidine (Pent; 10 μM). **e**, Mitochondrial translation response to inhibition of mitochondrial import with CCCP, measured by northern blotting for footprints (see **b**). **f**, Fold change in synthesis measured by cytoribosome profiling of nuclear-encoded mitochondrial mRNA-specific translational activators (colour-coded by mRNA target). For each mitochondrial mRNA, the names of the known translational activators are listed.

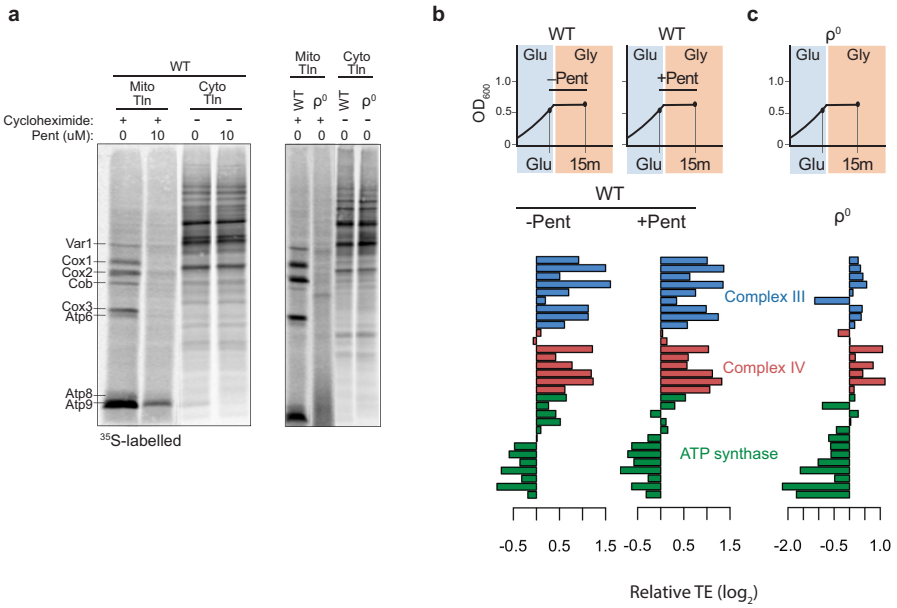

Extended Data Figure 9 | Cytosolic OXPHOS translation response is independent of mitochondrial gene expression. a, Metabolic labelling to measure mitochondrial translation (Mito Tln), detectable only in the presence of CHX, and cytosolic translation (Cyto Tln). Samples generated in the absence of CHX were diluted 15-fold before loading the gel compared to samples generated with CHX. Mitochondrial translation products are labelled. **b**, **c**, Full data set for experiment presented in Fig. 4d, e, showing fold changes in translation efficiency of all nuclear-encoded complex III, complex IV, and ATP synthase subunits measured by cytoribosome profiling without (−Pent) or with (+Pent) inhibition of mitochondrial translation (**b**) and in ρ^0 cells (**c**), which have neither mitochondrial translation nor functional OXPHOS complexes.

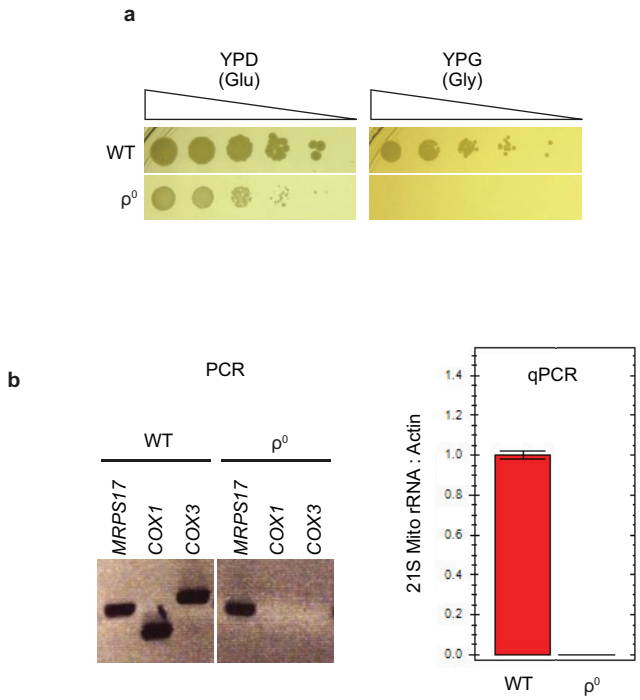

Extended Data Figure 10 | Verification of mtDNA loss in ρ^0 strain. **a**, Spot tests verifying that the ρ^0 strain generated by overnight growth in ethidium bromide (see Methods) cannot respire (no growth on YPG). **b**, PCR (left) and qPCR (right) verifying loss of mitochondrial-encoded genes *COX1*, *COX3*, and the 21S mitochondrial rRNA gene. *MRPS17* is nuclear-encoded. Bars show s.e.m. for technical triplicates.